Surface and edge quality variation in precision machining of single crystal and polycrystalline materials

S Min[1]*, D-E Lee[1], A de Grave[2], C M De Oliveira Valente[3], J Lin[1], and **D A Dornfeld[1]**
[1] Laboratory for Manufacturing Automation, University of California, Berkeley, USA
[2] Laboratoire Sols-Solides-Structures, Domaine Universitaire, Grenoble, France
[3] Nucleus of Advanced Manufacturing, University of Sao Paulo, Sao Carlos, Brazil

The manuscript was received on 22 December 2004 and was accepted after revision for publication on 5 October 2005.

DOI: 10.1243/095440506X77599

Abstract: The surface and edge quality of single-crystal and polycrystalline copper workpieces has been observed to vary significantly as a function of crystallographic orientation. On the precision scale, the chip formation process is influenced by the microstructure of the material, such as grain boundaries and grain orientation in polycrystalline materials, and crystallographic orientation in single-crystal materials. Such variation in the microstructure has a significant effect on the resulting surface, edge, and burr topography.

Keywords: micromachining, crystallographic orientation effect, surface and edge quality

1 INTRODUCTION

In the manufacturing of microscale structures, microelectromechanical system (MEMS) fabrication techniques based on traditional semiconductor fabrication processes such as lithography and etching have been preferred because they are proven technologies for industry application. However, inherent characteristics of these fabrication techniques limit material selection, process reliability, and degree of design latitude. Additionally, the environmental hazards associated with these processes are a significant issue, requiring major capital investment for set-up (including adequate environmental safeguards) and maintenance of production facilities.

Scaled-down versions of traditional mechanical manufacturing processes such as drilling and milling may serve as viable complementary processes to existing MEMS fabrication techniques. However, many challenges remain for the micromechaical machining process (hereafter referred to as micromachining) to be implemented at the production level. Schaller *et al.* [**1**] performed micromilling of microgrooves on brass and stainless steel with a width of less than 50 μm and found aspect ratio effects of tool edge radius to the depth of cut as a noticeable difference between conventional machining and micromachining (Fig. 1).

However, this effect can also be observed in macroscale conventional machining with negative rake angle tools. In fact, the experiments of Schaller *et al.* demonstrated that characteristics such as edge quality variation and the burr formation mechanism in particular were similar to those found in conventional machining. Lee *et al.* [**2**] repeatedly demonstrated these same results. Nevertheless, in microscale fabrication and ultraprecision machining, small changes in edge and surface quality can be manifested as process-induced defects such as burrs or breakout, causing an entire product to be discarded since post-processing operations (such as deburring and edge finishing) may be too expensive or impractical to implement.

It is important to distinguish micromachining as an entirely different process from macroscale machining which possesses several distinct characteristics that affect the final process outcome. For the purpose of this work, micromachining is defined as 'machining with a tool whose dimension is of the order of the average grain size of the workpiece material and/or the specific feature being generated' or 'machining with a tool whose dimension is small enough to lose isotropic homogeneity with respect to the workpiece material', rather than machining with a tool dimension less than a specific

**Corresponding author: Department of Mechanical Engineering, University of California at Berkeley, 5114 Etcheverry Hall, Berkeley, CA 94720-1740, USA. email: skmin@lma.berkeley.edu*

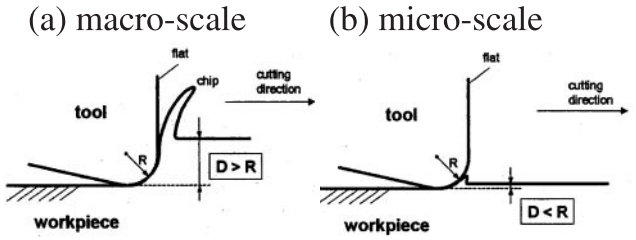

Fig. 1 Schematic view of the cutting edge–workpiece interaction at a given radius of curvature of the cutting edge (r is the radius of curvature of the cutting edge; d is the depth of cut) [**1**]

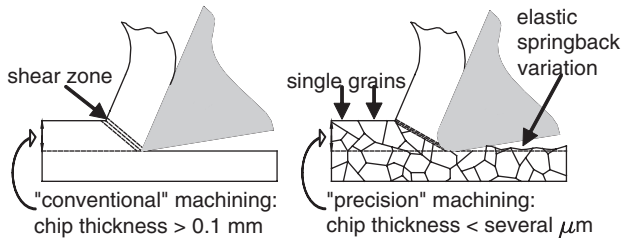

Fig. 2 Relative scale comparison of conventional versus precision cutting processes [**6**]

size, a concept that has been commonly used in many publications [**1–5**].

In ultraprecision machining, the undeformed chip thickness can be of the order of a few microns or less. On these length scales, the surface and edge condition of machined features and the fundamental mechanism for chip formation are much more intimately affected by the material properties and microstructure of the workpiece material, such as ductile–brittle behaviour and microtopographical features such as voids, secondary phases, and interstitial particulates [**6**]. When cutting single-crystal materials, the specific orientation of the material with respect to the cutting direction will have a significant impact on the resulting surface and edge condition. Likewise, when cutting polycrystalline materials with these small undeformed chip thicknesses, the material removal mechanism can be highly influenced by individual grains and their respective orientations. Therefore, unlike conventional metal cutting, the cutting mechanism in ultraprecision machining is more influenced by the crystallography and active dislocation slip systems within the workpiece (Fig. 2).

Previous work performed by Ueda and Iwata [**7**] demonstrated a significant variation in cutting force and chip topology in microcutting of brass as a function of crystallographic orientation. Subsequent work by Sato *et al.* [**8**] also indicated a significant variation in surface finish, chip topology, and cutting force during the machining of single-crystal aluminium. Similar work by Yuan *et al.* [**9**] has demonstrated variation in surface finish and cutting force in continuous face turning of single-crystal copper. To complement the above work, this paper focuses specifically on variation in the observed surface and edge condition of precision machined workpieces, including observation of burrs as a function of crystallographic orientation.

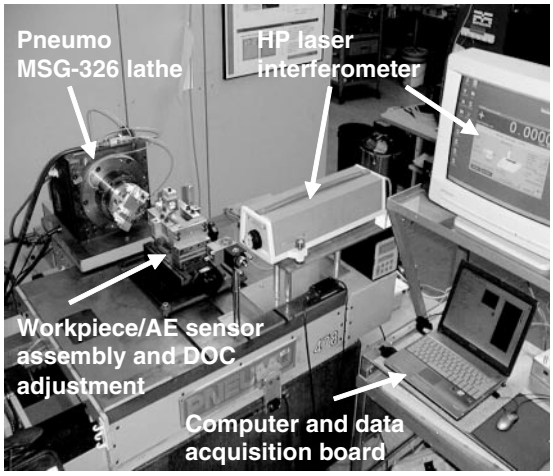

Fig. 3 Flycutting system set-up

2 EXPERIMENTAL SET-UP

Two types of material, single-crystal and polycrystalline oxygen-free high conductivity (OFHC) copper, were used for this work. The single-crystal copper workpieces were grown by the Bridgeman technique and rated at 99.999 per cent purity, with dimensions of 12.7 mm in diameter and 1 mm in thickness. Three single-crystal orientation copper workpieces ($\langle 100 \rangle$, $\langle 110 \rangle$, and $\langle 111 \rangle$) were tested. The polycrystalline workpieces used were nominally OFHC copper flats of 63.5 mm diameter which were cold worked at 60 per cent and subsequently recrystallized at 830 °C for different time durations (20–60 min), resulting in various grain sizes from approximately 0.1 to 4 mm. The OFHC Copper flats were subsequently diced into 10 mm square pieces.

The machine tool used in this set-up was a modified Rank Pneumo MSG-326 precision lathe equipped with a Professional Instruments Blockhead 4R air bearing spindle and precision air-bearing lays (Fig. 3). A HP laser interferometer was used to set the tool infeed position with a precision of approximately 0.1 μm. Spindle speed was measured with a Heidenhain rotary encoder with a precision of 1 r/min.

The flycutting operation consisted of mounting a single-crystal diamond tool of 0.274 mm nose radius (10° rake and 12.5° clearance) directly on to the spindle at a distance of 47.5 mm from the centre. Spindle speed was set in most cases to 420 r/min, hence generating a surface cutting speed of 2.1 m/s.

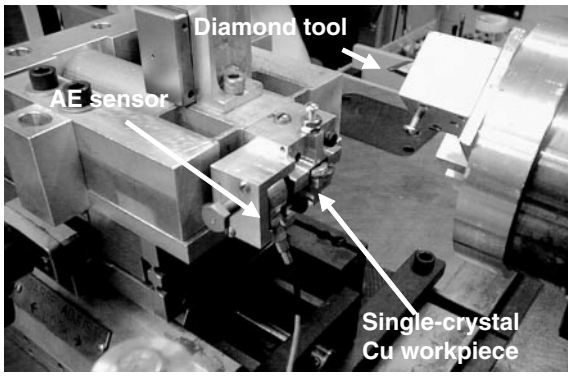

Fig. 4 Workpiece–AE sensor assembly set-up

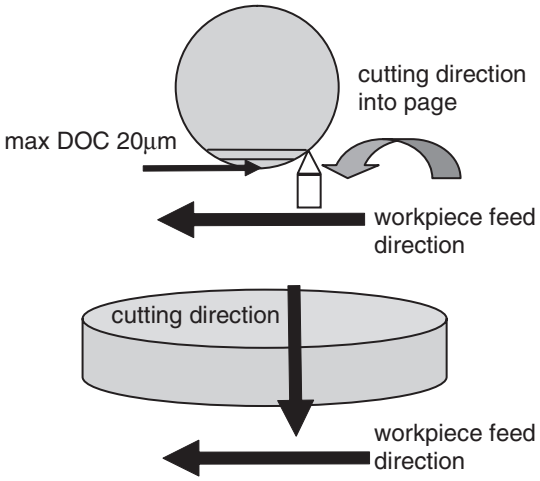

Fig. 5 Schematic diagram of the cutting direction and tool–workpiece relation

A constant cross-feed of 13.3 μm/rev was chosen for all experiments in order to maintain similar chip geometries and theoretical surface finishes across all experiments. Theoretical values of surface finish were calculated with R_{th} (peak–valley finish) of about 80 nm and R_a (centre-line average surface finish) of 20 nm.

The workpiece was held in place by a sample holder shown in Fig. 4. The height of the workpiece was adjusted using shims such that the tool cut parallel to the workpiece axis. A DECI SE900-MWB acoustic emission (AE) sensor was used as a contact sensor for tool positioning. The AE sensor was positioned directly on the workpiece holder and coupled with mineral oil to minimize signal attenuation. For zeroing the tool position for each machining pass, the workpiece was slowly advanced towards the rotating tool until a slight AE signal was observed, indicating contact of the order of 1 μm in depth of cut (DOC). After using the AE sensor as a contact sensor to 'zero' the tool with respect to the workpiece, a single pass with maximum nominal DOC of 20 μm (corresponding to a chord length of approximately 1 mm on the workpiece) was taken,

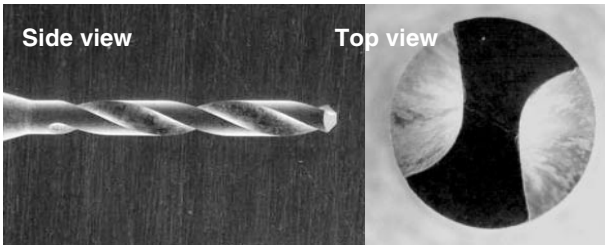

Fig. 6 Pictures of a drill of diameter 250 μm

resulting in a DOC gradient from nearly zero to a maximum of 20 μm in the middle of the machining pass. A second final pass of 20 μm was subsequently taken, in order to maintain a constant DOC across the machined surface (Fig. 5).

In order to investigate the influence of individual grains on burr formation in drilling, a series of drilling experiments were conducted on a Mori-Seiki TV-30 computer numerical-controlled tapping centre with uncoated WC drills, 250 μm in diameter (Fig. 6). Polycrystalline OFHC copper workpieces with thicknesses of 130, 250, and 375 μm were used. The feed and spindle speed were varied from 0.5 to 10 mm/min and from 6000 to 8000 r/min respectively. Oil lubricant was applied manually for both lubrication and cooling.

3 RESULTS

3.1 Precision flycutting results

For the machining of the ⟨100⟩ copper workpiece the tool cuts in an approximate straight path parallel to the ⟨100⟩ direction with the machined surface along the {100} plane. A Wyko NT3300 white-light interferometry surface profilometer was used to measure surface finish. A smooth surface finish with an average of 23.1 nm R_a was obtained. As seen from Fig. 7(a), the resulting edge shows only a slight burr extending approximately 5 μm from the edge, which is mostly uniform and does not exhibit any breakout. The collected chip, shown in Fig. 7(b), is mostly uniform in shape.

The ⟨100⟩ crystal was then cut across the {110} plane (with the same ⟨100⟩ cutting direction) by rotating the crystal in the sample holder by 45°. Figure 8 shows the SEM and Wyko surface images and collected chip. A significant change in the burr height and geometry was found for this case, with the presence of relatively large burrs still attached to the edge. The average surface finish increased to about 30.4 nm R_a. Also, a significant change in the chip topology was observed, with the edges of the chip exhibiting a feathered look (Fig. 8(b)).

A simple explanation for this variation in chip topology and surface finish is offered as follows.

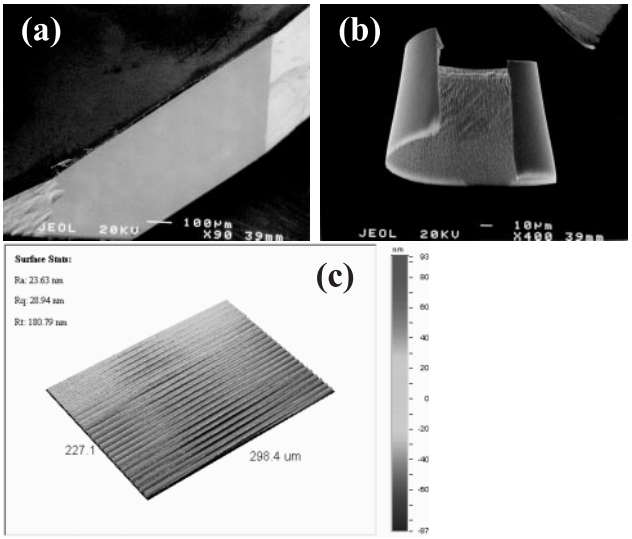

Fig. 7 (a) Scanning electron microscopy (SEM) surface image, (b) collected chip, and (c) Wyko surface image for a ⟨100⟩ crystal ({100} plane)

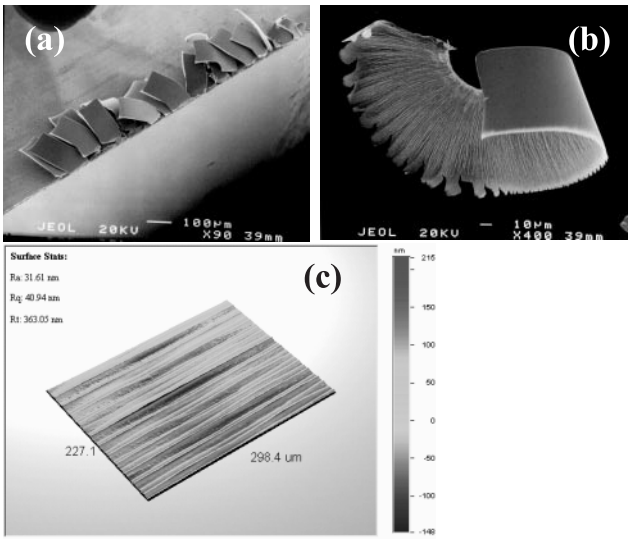

Fig. 8 (a) SEM surface image, (b) collected chip, and (c) Wyko surface image for a ⟨100⟩ crystal ({110} plane)

Copper has a face-centred cubic structure, with a ⟨110⟩–{111} slip system. Ductile plasticity and chip formation in machining is usually accomplished with the movement of dislocations along the preferred {111} slip planes in the ⟨110⟩ directions in the shear zone ahead of the tool. Figure 9 shows the interaction of the tool with the workpiece in the orientations shown in Figs 7 and 8, with the potentially active slip systems represented by the pyramid (each face of the pyramid representing a {111} plane with each vertex representing a ⟨110⟩ direction). It is assumed that the tool acts to force most dislocation movement in an upward fashion away from the machined workpiece, and few dislocations travel

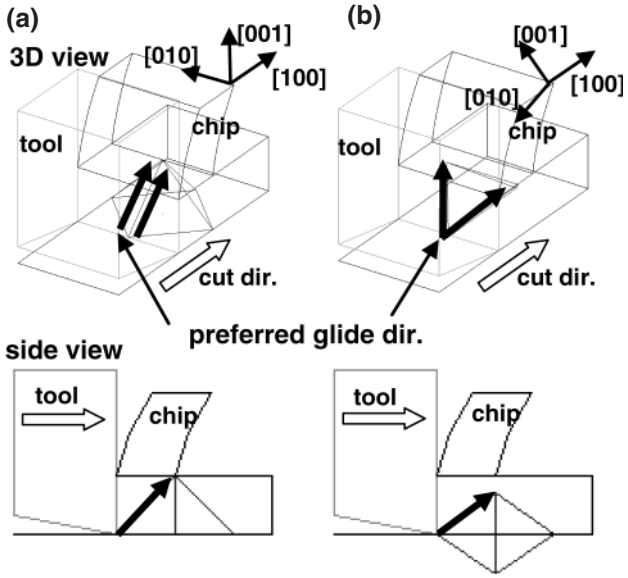

Fig. 9 (a) Slip system–tool interaction for the ⟨100⟩ direction ({100} plane); (b) slip system–tool interaction for the ⟨100⟩ direction ({110} plane)

downwards back into the machined surface. In the case shown in Fig. 9(a) for machining in the ⟨100⟩ direction along the ⟨100⟩ face, the dislocations on adjacent slip systems (designated as solid arrows) glide parallel to one another, hence allowing for relatively easy chip formation and a smooth surface finish. This behaviour is reflected in the smooth laminar appearance of the chip in Fig. 7(b).

However, in the case of Fig. 9(b) for machining in the ⟨100⟩ direction along the ⟨110⟩ face, dislocations gliding on the same {111} plane collide with one another, making it relatively more difficult (and more energy consuming) for chip formation to take place. The interference between adjacent dislocations is manifested in both the chip topology shown in Fig. 8(b) (which shows the chip as having a distorted topology with a significant amount of edge feathering), and the increase in roughness of the surface finish. Hence, for each single-crystal workpiece, there exists certain crystallographic orientations which are more favourable for relatively easy dislocation glide and chip formation than other orientations. However, the exact dependence of burr formation on crystallographic orientation has yet to be established from a theoretical modelling standpoint and remains as a topic of future research.

For machining the ⟨110⟩ workpiece shown in Fig. 10, the tool cut in the ⟨110⟩ direction with the machined surface along the {100} plane. As seen from Fig. 10(a), the resulting edge has a slight burr about 10 μm in height with no breakout observed. The presence of voids and *in-situ* defects in this particular workpiece caused the surface finish to

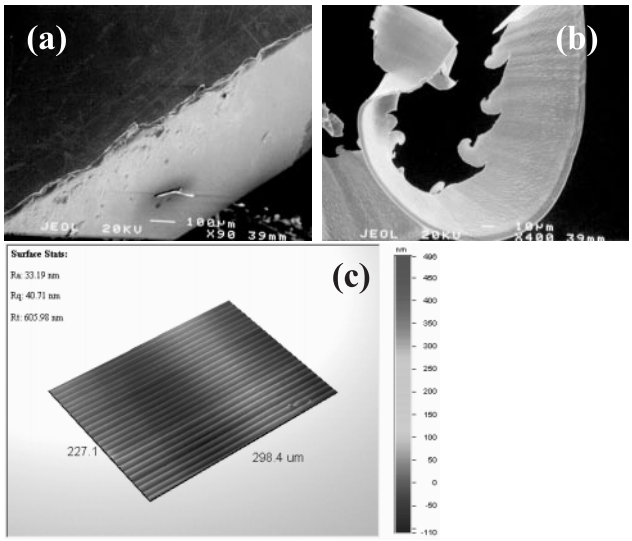

Fig. 10 (a) SEM surface image, (b) collected chip, and (c) Wyko surface image for a ⟨110⟩ crystal ({100} plane)

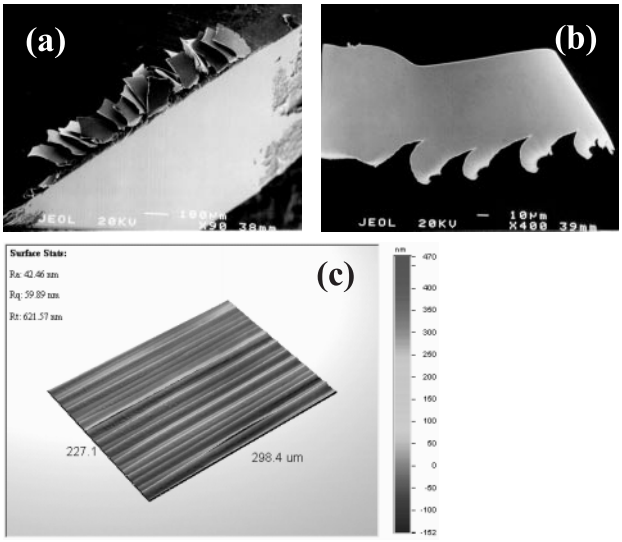

Fig. 11 (a) SEM surface image, (b) collected chip, and (c) Wyko surface image for a ⟨110⟩ crystal ({111} plane)

degrade significantly in certain parts of the machined surface, but an average surface finish of 32.6 nm R_a was measured in the regions without defects. The collected chip exhibited a slightly ruffled appearance with some edge feathering (Fig. 10(b)). The ⟨110⟩ crystal was then cut across the {111} plane (maintaining the same ⟨110⟩ cutting direction) by rotating the crystal in the sample holder by 54.7°. A very significant change in the edge condition was observed, with the presence of breakout and large burrs approximately 200 μm in length still attached to the surface (Fig. 11(a)). The surface finish was observed to increase slightly to 37.1 nm R_a, with a slight increase in the amount of

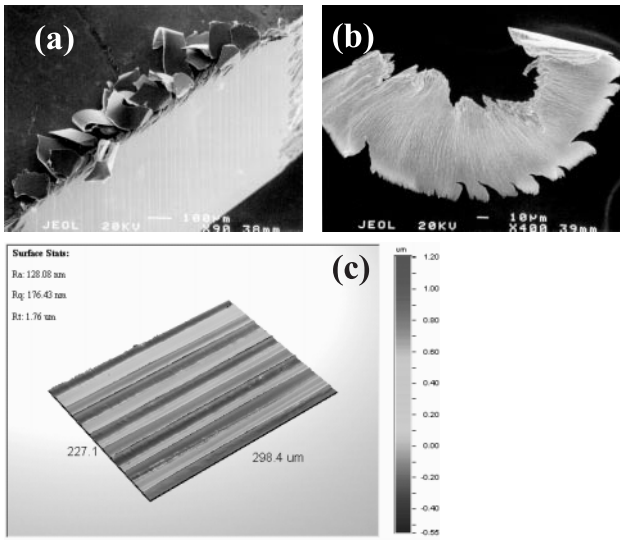

Fig. 12 (a) SEM surface image, (b) collected chip, and (c) Wyko surface image for a ⟨110⟩ crystal ({110} plane)

feathering in the chip edge (Fig. 11(c)). The ⟨110⟩ crystal was then rotated in the sample holder by 90° from its original orientation such that the machined surface was aligned along the {110} plane. Burrs of similar size to the previous case in Fig. 11 were found (Fig. 12(a)), with the collected chip shown in Fig. 12(c) exhibited a greater amount of distortion and ruffling compared with previous machining cases. A significant increase in the surface finish was found (Fig. 12(c)), with an average surface finish value of 130 nm R_a being measured, indicating that this orientation is not favourable when a combination of good surface finish and smooth edge quality is desired. The key issue of note is that rotating the ⟨110⟩ workpiece to different orientations can bring about a very significant change in the burr geometry, chip topology, and surface finish.

Figures 13 and 14 show SEM pictures of the edge for a ⟨111⟩ workpiece. Figure 13 shows the edge and surface of the workpiece machined along the {110} plane in the ⟨111⟩ direction, with a resulting surface finish of 25.6 nm R_a. An extremely smooth and homogenous chip was obtained for this machining case (see Fig. 13(c)). After machining in this configuration, the workpiece was rotated by 30°, and Figs 14(a) and (c) shows the edge and surface respectively of the workpiece being machined along the {211} plane. An average surface finish of about 26.2 nm R_a was measured, with the collected chip exhibiting an increased amount of distortion and ruffling (Fig. 14(b)). While the first cutting case in Fig. 13 shows only a slight burr (about 5 μm in height) extending from the edge with several large burrs attached, the second case in Fig. 14 shows

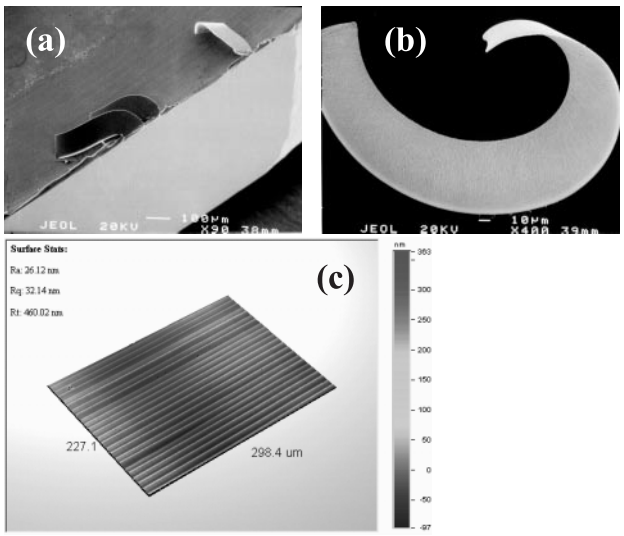

Fig. 13 (a) SEM surface image, (b) collected chip, and (c) Wyko surface image for a ⟨111⟩ crystal ({110} plane),7pc6.96,41pc10,57pc

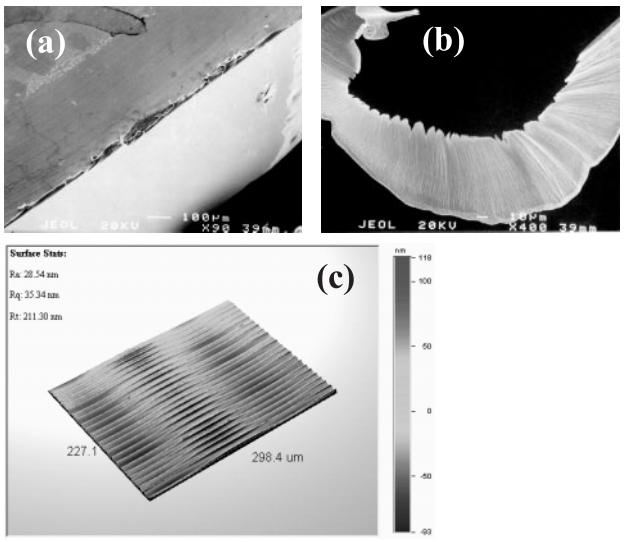

Fig. 14 (a) SEM surface image, (b) collected chip, and (c) Wyko surface image for a ⟨111⟩ crystal ({211} plane)

a continuous burr with an increased amount of edge distortion.

As a further test, the ⟨110⟩ workpiece was rotated to several specific orientations as shown in Fig. 15 for different cutting speeds. The first column of Fig. 15 shows an initial series of cuts that were made at a cutting speed of 2.1 m/s on the ⟨110⟩ workpiece at four orientations where the machined surface was parallel to the {100}, {322}, {111}, and {110} planes respectively. The cutting speed was increased to 6.8 m/s (1330 r/min), and the resulting surfaces are shown in the second column of Fig. 15. A significant variation in the edge condition was found with significantly fewer burrs found at the {100}, {322},

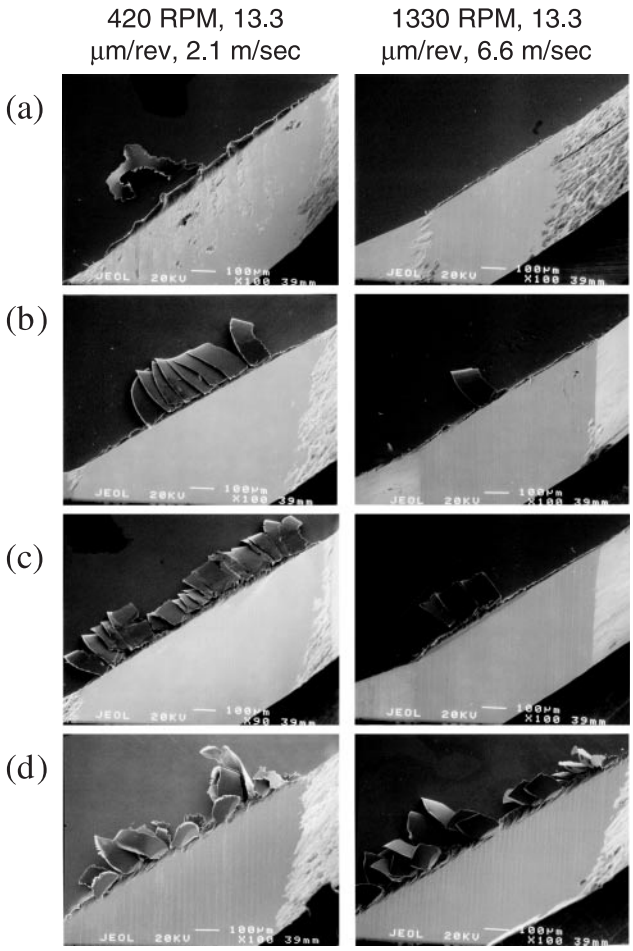

Fig. 15 SEM images for a ⟨110⟩ crystal: (a) {100} plane; (b) {322} plane; (c) {111} plane; (d) {110} plane

and {111} orientations at higher cutting speeds. Higher speeds also led to a slight decrease in overall burr height.

Figure 16 shows two polycrystalline copper workpieces (average grain diameter, 250 μm) machined with the same experimental parameters as for the single-crystal experiments. After machining, the resulting surfaces were chemically etched to reveal the underlying grain structure. In both cases, the resulting edge topology and burrs varied significantly as a function of grain orientation, with each grain exhibiting a different burr height.

3.2 Microdrilling results

Drilling burrs depend on many process parameters, with feed rate as a dominant factor [**10–14**]. In general, a crown burr forms at higher feed rates, and a uniform burr forms at lower feed rates in most ductile metals (Fig. 17). The boundary between these two distinctive burr types mostly depends on material properties.

The maximum feed rate used during the microdrilling experiments was 10 mm/min. During the

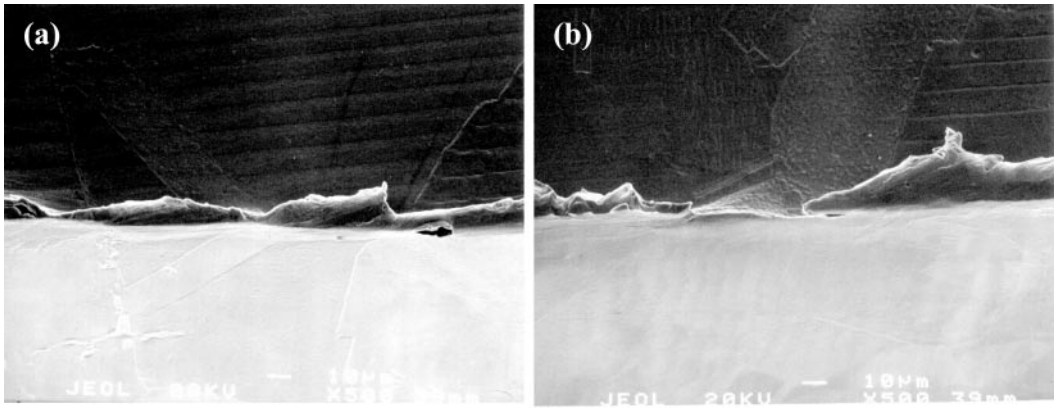

Fig. 16 SEM images of various burr heights in polycrystalline copper workpieces

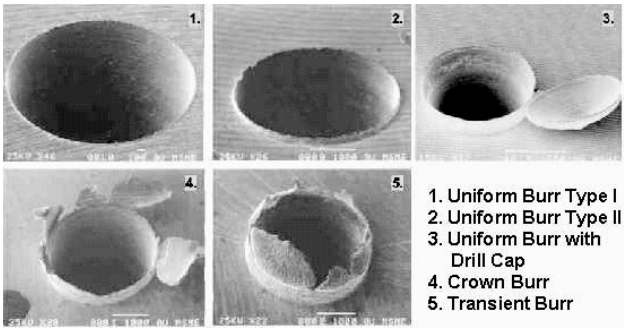

Fig. 17 Typical drilling burrs in ductile metals [**13**]

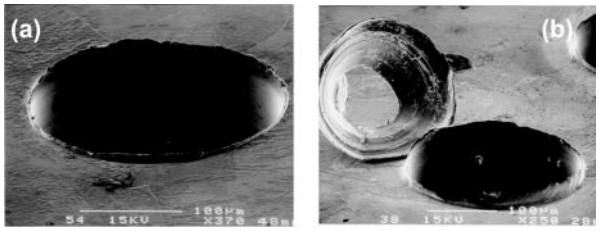

Fig. 18 Burr types found in microdrilling: (a) uniform burr (10 mm/min; 8000 r/min); (b) uniform burr with a drill cap (5 mm/min; 8000 r/min)

experiments, no crown burrs were observed. Typical burr types found were the uniform burr and uniform burr with a drill cap, as shown in Fig. 18. The shapes of the burrs were not entirely unlike those found in conventional macroscale drilling, indicating that the burr formation mechanism is similar to that in conventional drilling. During the burr initiation stage, as the drill advances, the plastic zone at the centre of the drill tip reaches the exit surface of the workpiece. The thin layer of the plastic zone in the uniform burr does not have enough support to be cut by the drill so that, during the development stage, very little cutting near the centre of the drill occurs, and yet cutting is still dominant near the edge of the drill. The plastic zone that initially

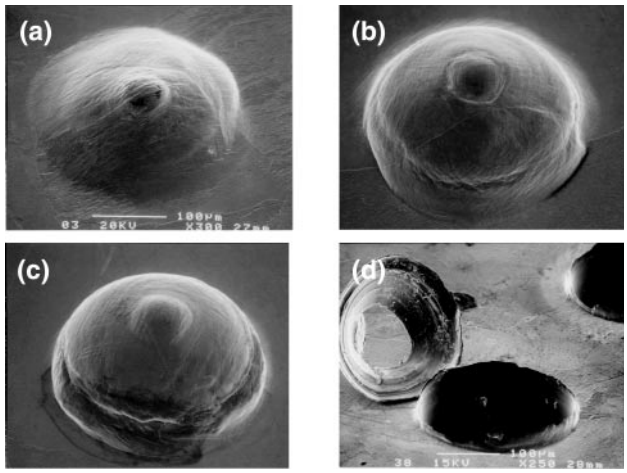

Fig. 19 Burr formation processes: (a) plastic zone expanding from the centre to the edge; (b) initial fracture at the edge; (c) fracture spreading along the edge; (d) final burr with a drill cap

formed near the centre of the drill area then expands to the edge of the drill (Fig. 19(a)). With expansion of the plastic zone and edge cutting, initial fracture occurs at the edge of the drill and creates a uniform burr (Fig. 19(b)). Because of imperfections in the process, initial fracture does not occur at some of the edges and it leads to the formation of a drill cap, as shown in Fig. 19(d).

Overall aspects of microscale burr formation are similar to macroscale burr formation, and yet it was observed that burr height and topology varies as a function of grain orientation. Since the tool diameter used was of the order of grain size, in most cases, the cutting physics taking place at the tool edge varies as the tool moves from one grain to another. Because the cutting direction of drill changes continuously during the process, and individual grain orientations are not known in advance, it is very difficult to establish a clear relationship between these two factors for drilling. However, Fig. 20 clearly shows that one grain orientation favours a particular cutting

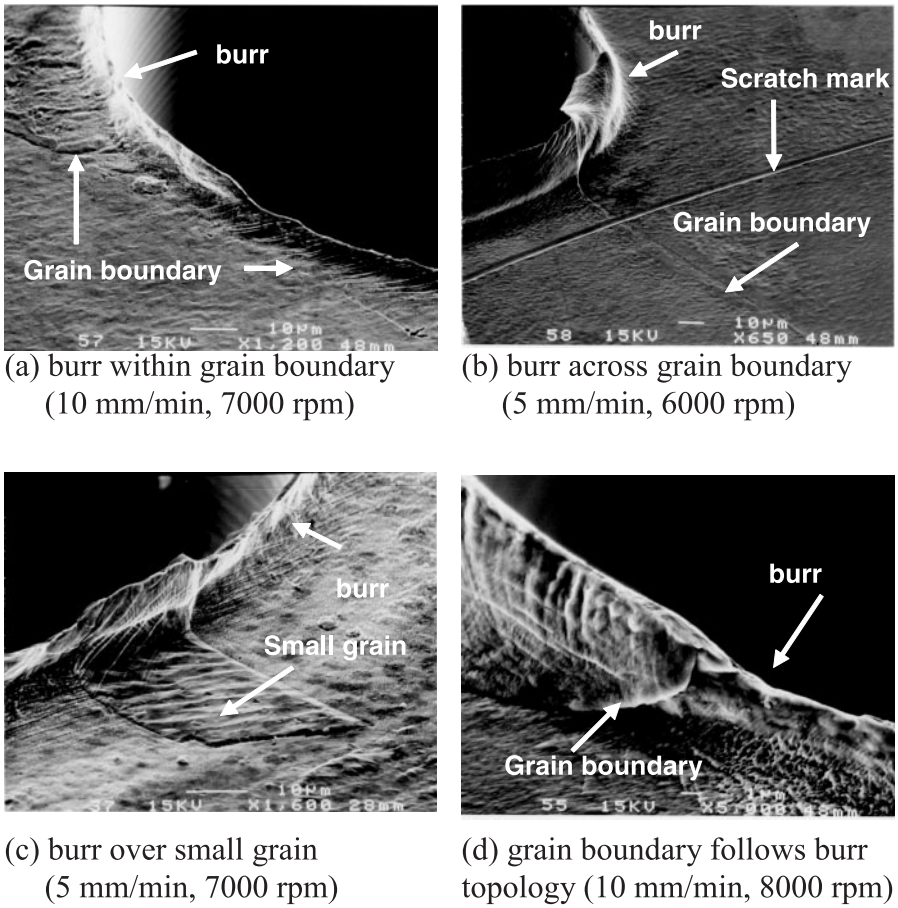

(a) burr within grain boundary (10 mm/min, 7000 rpm)

(b) burr across grain boundary (5 mm/min, 6000 rpm)

(c) burr over small grain (5 mm/min, 7000 rpm)

(d) grain boundary follows burr topology (10 mm/min, 8000 rpm)

Fig. 20 Microdrilling burr formation across different grains

direction, which leads to a ductile-like cutting mode and in turn a larger burr.

4 CONCLUSION

A significant variation between the surface and edge condition and the crystallographic orientation has been found in the precision machining of single-crystal and polycrystalline copper. Certain crystallographic orientations were found to yield a rougher surface finish, as well as significant burrs and breakout at the tool exit edge. Some key observations were made for machining in particular crystallographic orientations.

1. Machining of the ⟨100⟩ and ⟨111⟩ workpieces tended to yield the smoothest surface finish ranging from 20 to 30 nm R_a, whereas the ⟨110⟩ crystal orientation with a {110} machined plane exhibited the roughest surface finish of 130 nm R_a.
2. The ⟨100⟩ and ⟨110⟩ workpieces exhibited the greatest amount of variation in burrs and breakout at the exit edge and chip topology as a function of the angular orientation of the workpiece, corresponding to a variation in interaction between the tool and activated slip systems.

It was also found that grain orientation affected burr formation in the drilling of polycrystalline copper. A single material may produce a ductile-like cutting mode in one grain and brittle-like cutting in another, indicating that favourable and non-favourable cutting orientations for good surface and edge condition exist as a function of crystallographic orientation. These observations demonstrate the importance of further research in this field.

The present authors hope this study will attract further attention to the influence of workpiece microstructure on micromachining. Many issues still remain and need to be investigated further in order to develop micromachining as a viable supplement to existing MEMS fabrication processes. Among those are the following:

(a) further refined testing of other crystallographic orientations to determine the effect on the surface and edge condition;
(b) investigation of burr formation in other micromachining processes, such as micromilling;

(c) establishing analytical relationships between crystallographic orientation, cutting direction, and the resulting surface and edge quality.

REFERENCES

1 **Schaller, Th., Bohn, L., Mayer, J.,** and **Schubert, K.** Microstructure grooves with a width of less than 50 μm cut with ground hard metal micro end mills. *Precision Engng*, 1999, **23**, 229–235.

2 **Lee, K., Ahn, S., Dornfeld, D. A.,** and **Wright, P. K.** The effect of run-out on design for manufacturing in micromachining process. In Proceedings of the ASME International Mechanical Engineering Congress and Exposition, New York, USA, November 2001 (American Society of Mechanical Engineers, New York).

3 **Rahman, M., Kumar, A. S.,** and **Prakash, J. R. S.** Micro milling of pure copper. *J. Mater. Processing Technol.*, 2001, **116**, 39–43.

4 **Moriwaki, T., Sugimura, N.,** and **Luan, S.** Combined stress, material flow and heat analysis of orthogonal micromachining of copper. *Ann. CIRP*, 1993, **42**(1), 75–78.

5 **Weule, H., Schmidt, J., Hüntrup, V.,** and **Tritschler, H.** Micromilling of ferrous materials. *Prod. Engng*, 1999, **6**(2), 17–20.

6 **Moriwaki, T.** Experimental analysis of ultra-precision machining. *Int. J. Japan Soc. Precision Engng*, 1995, **29**(4), 287–290.

7 **Ueda, K.** and **Iwata, K.** Chip formation mechanism in single crystal cutting of β brass. *Ann. CIRP*, 1980, **29**(1), 41–46.

8 **Sato, M., Yamazaki, T., Shimizu, Y.,** and **Takabayashi, T.** A study on the microcutting of aluminum single crystals. *JSME Int. J. Ser. III*, 1991, **34**(4), 540–545.

9 **Yuan, Z., Lee, W., Yao, Y.,** and **Zhou, M.** Effect of crystallographic orientations on cutting forces and surface quality in diamond cutting of single crystal. *Ann. CIRP*, 1994, **43**(1), 39–42.

10 **Gillespie, L. K.** Burrs produced by drilling. Unclassified topical report BDX-613-1248, Bendix Corporation 1975.

11 **Miyake, T., Yamamoto, A., Kitajima, K., Tanaka, Y.,** and **Takazawa, K.** Study on mechanism of burr formation in drilling: deformation of material during burr formation. *J. Japan Soc. Precision Engng*, 1991, **57**(3), 485–490.

12 **Min, S., Kim, J.,** and **Dornfeld, D. A.** Development of a drilling burr control chart for low alloy steel. AISI 4118. *J. Mater. Processing Technol.*, 2001, **113**(1–3), 4–9.

13 **Min, S., Kim, J.,** and **Dornfeld, D. A.** Thrust force analysis of drilling burr formation using finite element method. In Proceedings of the Tenth International Conference on *Precision engineering*, Yokohama, Japan, 2001, pp. 169–173.

14 **Kim, J., Min, S.,** and **Dornfeld, D. A.** Optimization and control of drilling burr formation of AISI 304L and AISI 4118 based on drilling burr control charts. *Int. J. Mach. Tools Mf.*, 2001, **41**(7), 923–936.